Synthesis of the modeling and control systems of a tunneling accelerometer using the MatLab simulation

2002 J. Micromech. Microeng. 12 730

(http://iopscience.iop.org/0960-1317/12/6/302)

INSTITUTE OF PHYSICS PUBLISHING JOURNAL OF MICROMECHANICS AND MICROENGINEERING
J. Micromech. Microeng. **12** (2002) 730–735 PII: S0960-1317(02)34961-1

Synthesis of the modeling and control systems of a tunneling accelerometer using the MatLab simulation

Jing Wang, Yongjun Zhao, Tianhong Cui and Kody Varahramyan

Institute for Micromanufacturing, Louisiana Tech University, 911 Hergot Avenue, Ruston, LA 71272, USA

E-mail: tcui@coes.latech.edu

Received 18 March 2002, in final form 12 June 2002
Published 28 August 2002
Online at stacks.iop.org/JMM/12/730

Abstract
In this paper, we construct the function model of a tunneling accelerometer using MatLab Simulink. With small input signal approximation, the tunneling current and electrostatic actuator nonlinear blocks are analyzed and linearized. From the derived relation between open and close loop transfer functions, we synthesize a simple but effective way to design the control system. By choosing a control system, the accelerometer bandwidth is broadened and the damping is enhanced. The system stability, root locus, step response, gain and phase margins, and pole-zero distribution are all plotted and discussed. With the designed control and feedback systems, a close loop system is stable on both parameter disturbance and frequency response. Compared with the real system at 50 ng $Hz^{-1/2}$ noise level, we also present tunneling accelerometer characteristics, such as the exponential relationship between tunneling current and displacement change, time history record, dynamics and frequency response.

1. Introduction

Since the Nobel prize was awarded to Binnig and Rohrer in 1986 for building the first scanning tunneling microscope (STM) utilizing tunneling current, the possibility of producing a highly-sensitive tunneling displacement transducer has been actively explored. Several years after the advent of the first tunneling transducer [1], Waltman and Kaiser [2] and Kenny and Waltman [3] developed sensors with a displacement resolution approaching 10^{-4} Å $Hz^{-1/2}$. In electron tunneling transducers, a 1% change in the 1.5 nA current between tunneling electrodes corresponds to a displacement fluctuation of less than 0.1 Å. This high sensitivity is independent of the lateral size of the electrodes because the tunneling current occurs between two metal atoms located at opposite electrode surfaces. Due to their high sensitivity and miniature size, micromachined tunneling transducers make it possible to fabricate a high performance, small-sized, light mass, inexpensive accelerometer, which is in great demand in applications such as microgravity measurements, acoustic measurements, seismology and navigation.

Considerable research work on accelerometers [4–6] has been developed. However, most micromachined tunneling accelerometers still suffer the problem of enhancing resolution while broadening measurement bandwidth. Liu *et al* have developed a controller design by μ-synthesis [7], which has accomplished a high precision, wide-bandwidth micromachined tunneling accelerometer [8]. However, the method is complicated and frustrating, especially to new device designers, who intend either to devise innovative tunneling sensors or to reconstruct revised structures for better performance. Because their purpose is not to accommodate different sensors for mass production as in Liu's μ-synthesis method, a simple, effective and effortless design method is necessary. In this paper, a computer aided engineering (CAE) tool, MatLab Simulink, is chosen as a kind of technical computing language to model and simulate the function of the tunneling accelerometer. After approximation at small signal input, a simpler means to synthesis control systems is established. The designed transfer function is evaluated and compared with the real system. At the same time, we plot and discuss some simulation results of the mechanical performance, frequency response, system stability,

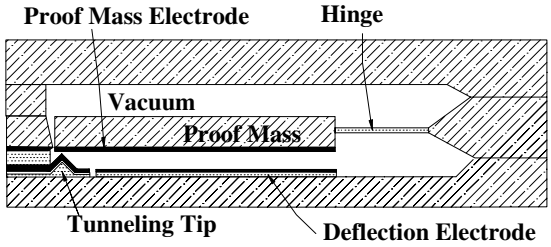

Figure 1. Schematic diagram of the cross section of a micromachined tunneling accelerometer.

time history, and dynamic range of tunneling accelerometers. Moreover, since the design and analysis of control systems can be done prior to the micromachining process, further research and mass production processes can be greatly expedited and streamlined.

2. Accelerometer structure

A typical tunneling accelerometer has mechanical components and three electrodes. The mechanical components comprise a fixed cantilever with a tunneling tip on the bottom and a mass component, or proof mass, suspended by a flexible hinge on the top. The electrodes include a tip electrode, proof mass electrode, and deflection electrode. The metal of the electrode is a layer of Au film, which is used because of its inert chemical characteristics as well as its relatively high work function. When operating, the accelerometer maintains a constant tip-to-proof mass distance by applying an electro static feedback force on the proof mass. The cross section of the tunneling accelerometer is illustrated in figure 1. Usually, at this constant distance operation point, the distance between the tip and proof mass electrode is about 10 Å and the tunneling current is about 1.5 nA. More detailed descriptions about the tunneling structures and operation principles can be found in [9–12]

3. Modeling

A MatLab Simulink model block diagram is constructed according to the accelerometer function structures, as shown in figure 2. The external acceleration Δa is applied on the proof mass and produces external force F_{ext}, which causes a displacement change, ΔX, between the tip and proof mass. In order to reduce the mechanical noise induced by thermal fluctuations, the tunneling transducer always operates at vacuum environment. Because of this, air damping can be omitted here. At force balance, there exists $F_{\text{spring}} = F_{\text{acceleration}}$, i.e. $K\Delta X = m\Delta a$, where m and K are the mass and stiffness of the proof mass, respectively. The K/m ratio is very important because it is inversely proportional to the sensitivity $\Delta X/\Delta a$ and it describes the proof mass natural frequency $\omega_{\text{n}} = \sqrt{K/m}$. The K value is mainly determined by the sensor's structure and size, which can be calculated either by mathematical methods for a simple structure or by simulation methods aided by ANSYS or other finite element analysis (FEA) software. It is easier to measure the natural frequency and we can always arbitrarily choose the mass of the proof mass to satisfy the need for the K/m ratio. Here the natural frequency is chosen as the input parameter for MatLab. In order to exhibit fast response time and large bandwidth, accelerometers require high natural frequencies. For better sensitivity and resolution performance, a small K/m ratio is necessary. The most challenging task for a tunneling accelerometer design is to enhance the resolution while broadening the bandwidth.

When a force is applied on a tunneling transducer, the distance change is $\Delta X = \frac{a}{\omega_{\text{n}}^2} \cdot T(s)$, where $T(s)$ is the proof mass frequency response, $T(s) = \frac{\omega_{\text{n}}^2}{s^2+2\omega_{\text{n}}\zeta\cdot s+\omega_{\text{n}}^2}$, with a second-order model simulation. The relation between damping ζ and quality factor Q is $\zeta \cdot Q = 1/2$. Because tunneling accelerometers are flexible and they often operate under a vacuum environment, it is easy to obtain a large Q value of 100 or more. Thus, the other purpose for control systems is to increase the damping to obtain $Q_{\text{eff}} = 0.707$. The change between the tip and the proof mass, ΔX, induces an exponential tunneling current $I = I_{\text{o}} \exp(-\alpha\sqrt{\Phi}\Delta X)$, where α is a constant, $\alpha = 1.025$ (Å^{-1} eV$^{-0.5}$) and Φ is the effective height of the tunneling barrier, whose typical value is 0.2 eV. The tip voltage, V_{tip}, from the sample resistor, is compared with reference voltage, V_{ref}, and amplified by a pre-amplifier thereafter. A control circuit with transfer function H_{c} is followed and the feedback voltage V_{fb} is produced. V_{fb} is input into an electrostatic actuator, which produces a feedback force F_{def}. Usually the actuator is a parallel capacitor whose force can be described as $F_{\text{def}} = \frac{\varepsilon S(V_{\text{hi}}+V_{\text{fb}})^2}{2(D+\Delta X)^2}$, where V_{hi} is a high dc voltage applied on the actuator to set the operation point, D is the nominal gap between the electrodes, ε is the permittivity, and S is the overlap area of the electrode pads. F_{def}, in turn, counterbalances the external force and keeps the tunneling tip at the operation point. The magnitude of the feedback voltage V_{fb} is proportional to the external force and is also called the output voltage V_{o}.

4. Small input analysis

In the simulation model of a tunneling accelerometer, there are two nonlinear blocks: one is the block between displacement changes and tunneling current, the other is the block between feedback voltage and deflection force. In order to synthesize the system, these two blocks are analyzed and linearized based on the practical small signal input.

The changes of tunneling tip–proof mass distance, ΔX, is about 10^{-3} to 10^{-1} Å, which has been measured by a laser vibration measurement system [4]. ΔX is small compared with the normal operation position of 10 Å. The current can be developed by Taylor series as $I = I_{\text{o}}(1 - a\sqrt{\Phi}\Delta X)$. Because the sample resistor R_1 is chosen such that the product of $I_{\text{o}}R_1$ is equal to the reference voltage V_{rf}, it is easy to obtain $V_1 = V_{\text{rf}} \cdot A \cdot \alpha\sqrt{\Phi} \cdot \Delta X$, where A is the amplitude of the pre-amplifier.

For an actuator, the electrostatic force is proportional to $(V_{\text{hi}} + V_{\text{fb}})^2$, that is $V_{\text{hi}}^2\left(1 + \frac{V_{\text{fb}}}{V_{\text{hi}}}\right)^2$. Because V_{hi} is a dc constant voltage, of about 100 V, and is much larger than V_{rf}, of several millivolts, the force can also be rewritten as being proportional to $V_{\text{hi}}^2 + 2V_{\text{hi}}V_{\text{fb}}$. The first item is to set the operation point and the second item is what we are concerned with. In other words, the change of the deflection force is proportional to

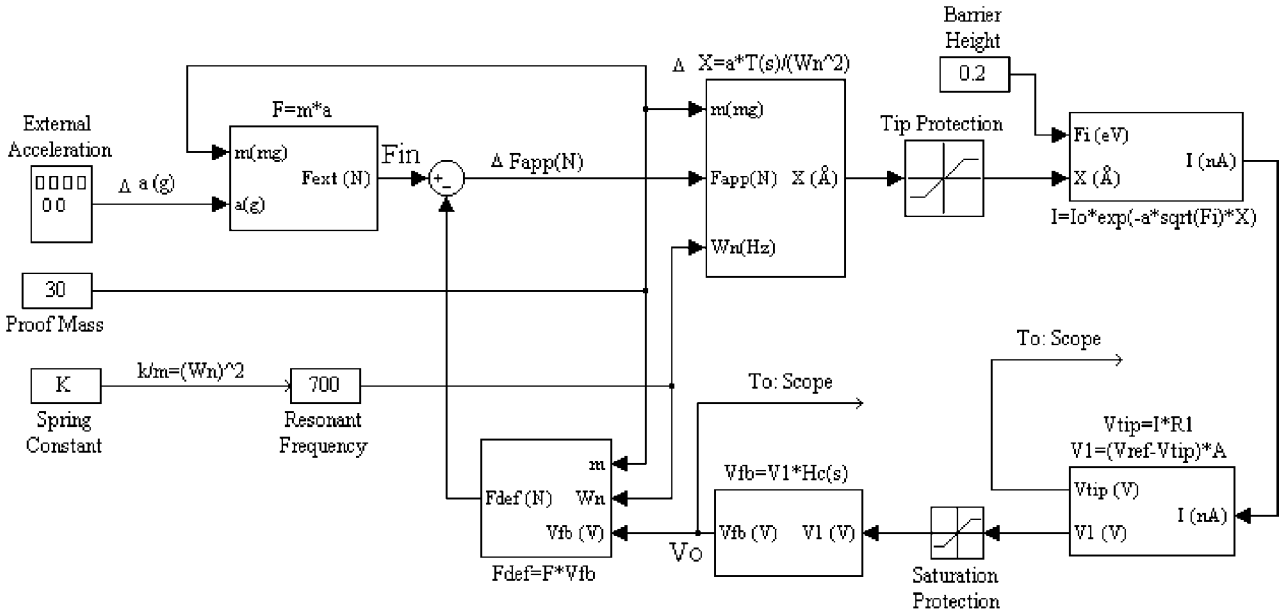

Figure 2. MatLab Simulink modeling block diagram.

$V_{\rm hi}V_{\rm fb}$ or, more simply, $F_{\rm def} = FV_{\rm fb}$, where F is the feedback factor. The value of F can be either estimated or tested in a real actuator. An estimated value is 1.5×10^{-5} (N V^{-1}) with an overlap area of 0.2×0.2 mm^2, a high voltage of 160 V, and a nominal distance of 2 μm.

With the above approximations, the nonlinear system now can be treated as a linear system at wavelet analysis. If $F_{\rm ext}$ is the input variable and $V_{\rm o}$ is output variable, the open and close loop transfer functions are $H_{\rm o} = H_{\rm c} \cdot \frac{V_{\rm rf} A\alpha\sqrt{\Phi}}{m\omega_{\rm n}^2} \cdot T(s)$ and $H = \frac{H_{\rm o}}{1+FH_{\rm o}}$, respectively.

5. Feedback and control design

When considering accelerometer resolution, a smaller natural frequency corresponds to a higher resolution. If the minimum resolved displacement is 10^{-2} Å, a 700 Hz proof mass should resolve 2 μg ($g = 9.8$ m s^{-2}) acceleration. The natural frequency of a proof mass cannot be chosen to be larger if a microgram resolution is wanted. The open loop property of tunneling accelerometers ceases to respond when the applied acceleration frequency is larger than the resonance frequency. The purpose for the control system design is to keep a highly sensitive and flexible tunneling proof mass while broadening the bandwidth. In addition, the transfer function, $T(s)$, is an unstable system. The control system needs to enhance the system stability so as to protect the tunneling tip against parameter disturbances and signal impulses. From the relation between H and $H_{\rm o}$, the control circuit with transfer function $H_{\rm c}$ should be synthesized so that the system transfer function H satisfies:

(1) the bandwidth of the system should be larger than the interested signal bandwidth;
(2) the system should be a stable system;
(3) the system needs to have a small response time so as to respond quickly enough;
(4) the system damping should be optimized so as to get instant response and protect tunneling tip;
(5) within interested frequency bandwidth, the sensitivity should be linear.

Using feedback theory, the bandwidth and stability can be enhanced by a factor of $|FH_{\rm o}|$. We hope to have $|FH_{\rm o}| \gg 1$, which means a large open operation amplifier in the system is necessary. On the other hand, the system transfer function can be simplified as $H \cong 1/F$ in a deep negative feedback system. In order to have a higher sensitivity, we prefer a smaller F value. The strategy to lower F is to lower the dc bias voltage, $V_{\rm hi}$. A large overlap area electrode and small nominal proof mass–deflection electrode distance are then often chosen. When starting to design, we first give a test $H_{\rm o}$, then evaluate the close loop transfer function H. If some conditions above are unsatisfied, we then change the controller $H_{\rm c}$ and give a correct test $H_{\rm o}$. All the synthesis processes are trial and evaluation. In fact, because of a large $|FH_{\rm o}|$ value, it is not difficult to find proper control system functions to meet the design requirements.

The changes of the normalized close loop transfer function H' dependent on the $|FH_{\rm o}|$ value are shown in figure 3. When the $|FH_{\rm o}|$ value increases, the system stability also increases. The ultimate goal for us is to make a damping factor of a close loop system $\zeta_{\rm eff} = 0.707$. A more detailed method of system damping chosen can be obtained from the step response of the normalized close loop system. As shown in figure 4, a system with a settling time of 0.1 ms and an overshoot of less than 1% is marked. By choosing feedback and a control system, the overall system can be both prompt to applied signals and stable with a proper damping ratio.

Without taking into account that it represents a significantly better methodology, this method presents an easy alternative for the new designer. Compared with the μ-synthesis method, our intended control system is not an exact and specific resolution for consideration. This relax requirement for the circuit is another advantage, though our

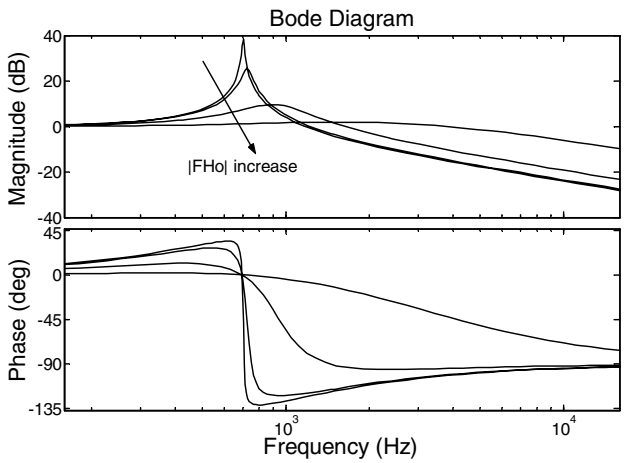

Figure 3. Diagram of the normalized close loop transfer function H' frequency response. The stability changes when the FH_o value increases.

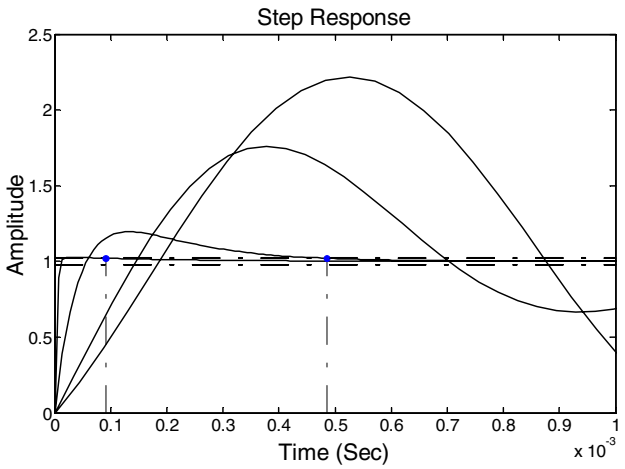

Figure 4. Step response of normalized close loop system.

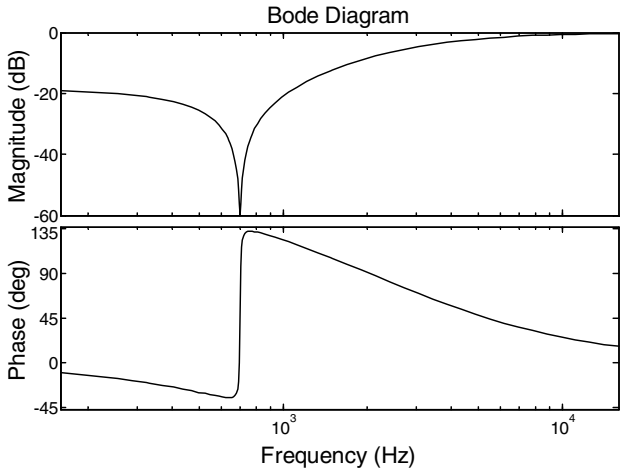

Figure 5. Bode diagram of synthesized control system.

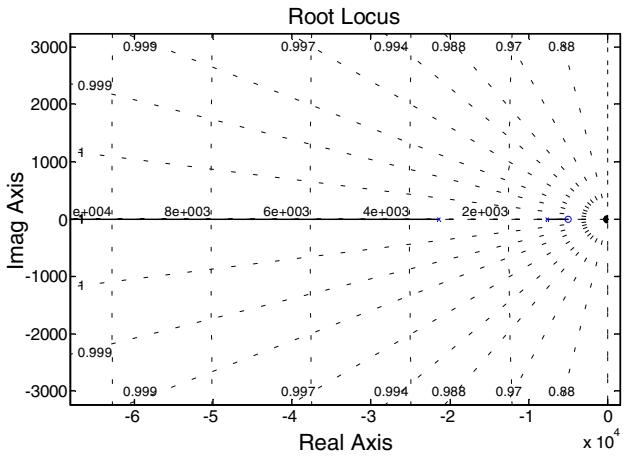

Figure 6. Root locus of the close loop system. The dotted line indicates the damping constant and response frequency.

designed control system is not as robust a controller as Liu's result. However, as shown in figure 5, our control system has a similar property with this μ-synthesis controller [7]. The very small low-frequency sensitivity (-20 dB) indicates that the close loop gain suffers minimally from open loop gain variation. At high frequencies, the applied signal receives phase compensation. At a bandwidth of 100 Hz to 1 kHz, the overshoot and noise are suppressed.

6. Simulation results and discussion

After synthesis, we evaluate the system transfer function satisfying the design criterion. The characteristics of one tunneling accelerometer are also simulated.

6.1. Close loop system evaluation

The gain and phase margin are parameters to describe the changes to make the system unstable. Systems with greater margins can withstand larger disturbances in system parameters before becoming unstable in close loop. By simulation, the gain margin is infinite and the phase margin is about 90°. The system is considerably stable.

The root locus is the locations of all possible closed loop poles, which shows how the closed loop stability changes when the amplitude of $H(s)$ changes. On the other hand, it is necessary to maintain a well-damped proof mass so as to avoid crashing when impulses or disturbances occur. From the phase margin obtained above, the damping ratio is about 0.9. When a disturbance occurs, the system does not cause fluctuations. To determine which part of the locus is acceptable, constant damping ratio lines are plotted in a root locus diagram. In figure 6, there are two sets of dotted lines: constant damping line (radiation) and response frequency line (perpendicular). In between the constant damping lines, the poles have larger ζ and all our possible system pole locations are on the $\zeta = 1$ line. From the selected frequency location, the response time can be estimated to be about $1/\omega$. Since all the poles are at the left half s-plane, the closed loop system will be stable.

6.2. Tunneling accelerometer function simulation

The controller system is proven to have been successively synthesized from the evaluation of transfer function

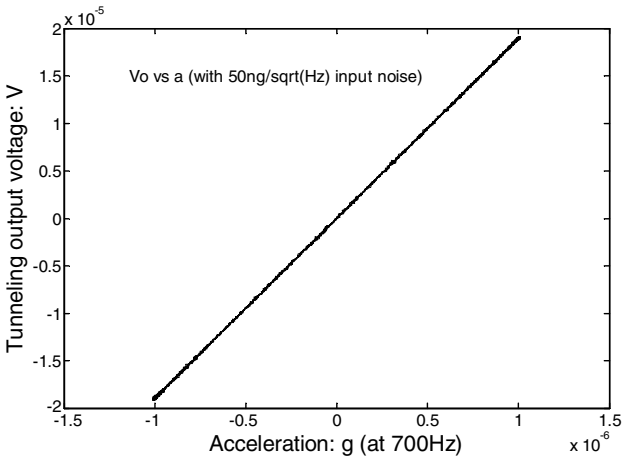

Figure 7. Transfer function and dynamic range of the tunneling accelerometer.

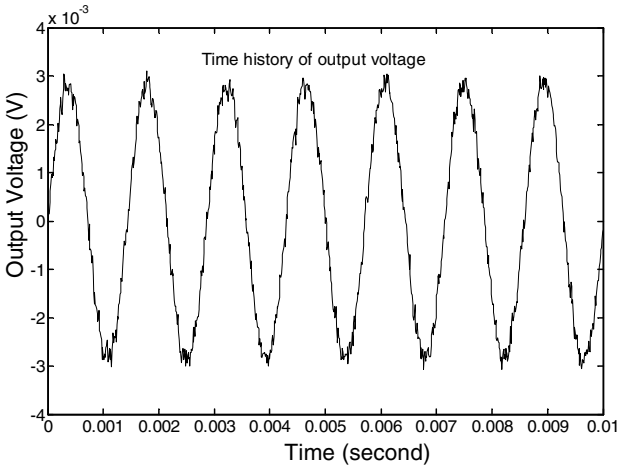

Figure 8. Time history of output voltage at 700 Hz, 1.5 μg acceleration and 50 ng Hz$^{-1/2}$ noise level.

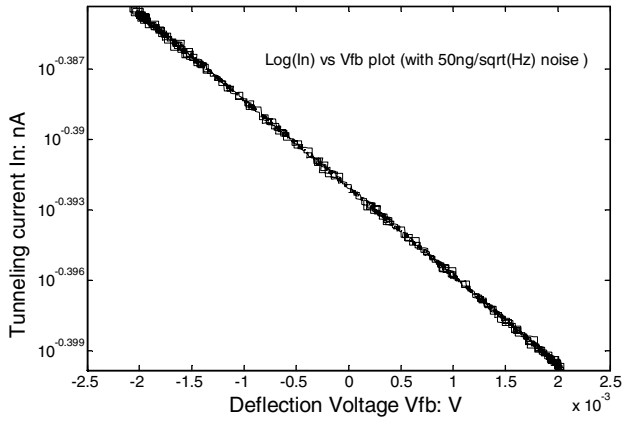

Figure 9. Tunneling current versus deflection voltage.

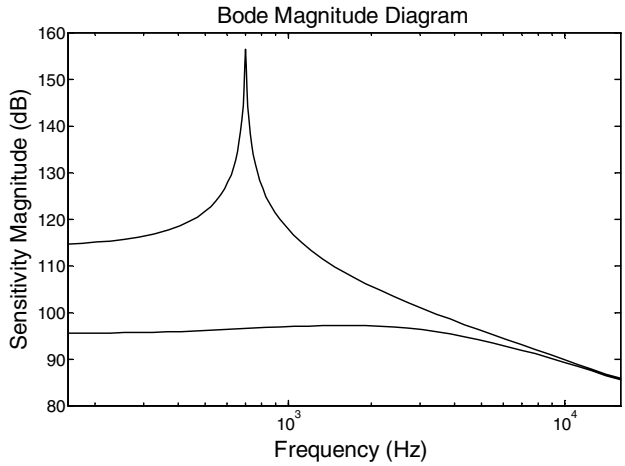

Figure 10. System sensitivity magnitude frequency responses of a tunneling accelerometer. The solid and dashed lines represent open and close loops, respectively.

characteristics and system stability. The functions of an accelerometer in an estimated noisy environment are then simulated. A well-estimated thermomechanical noise level for a tunneling sensor (equivalent to acceleration) is $\sqrt{\frac{4K_{\mathrm{B}}T\omega_{\mathrm{n}}}{m_{\mathrm{P}}Q}}$, where K_{B} is the Boltzmann constant, T is temperature, ω_{n} is the resonant frequency of the proof mass, m_{p} is the proof mass and Q is the mechanical quality factor [13, 14]. If we give Q as 50, the calculated value of the accelerometer noise is about 50 ng Hz$^{-1/2}$. Figure 7 shows the plot of feedback voltage dependent on input acceleration. The linearity is kept until the input is out of the dynamic range, which is about 1.2 mg and it is well matched with the measured value in [12]. The small dynamic range is the price of high sensitivity because of the small K/m value. When horizontal signals are under consideration and the whole system is put in the horizontal direction, the small dynamic range would not cause problems in the Earth's 1 g gravitational field.

Figure 8 shows the time history of accelerometer output at 700 Hz when the input acceleration is 1.5 μg and the white noise level is 50 ng Hz$^{-1/2}$. Figure 9 shows the semi log of current that depends on the bias deflection voltage to verify the tunneling effect. Without acceleration input and an open loop condition, the deflection voltage causes changes in tip current. The relation between semi log tunneling current and the deflection voltage fits the exponential tunneling equation very well and can also be used to measure tunnel barrier height, which is 0.2 eV as the MatLab Simulink designed. Finally, the sensitivity magnitude frequency responses of an open and close loop system are plotted in figure 10. Though the sensitivity of the close loop system is lowered at low frequency, the stability of the system is greatly enhanced and the sensitivity of voltage with respect to external force is about 95 dB up to 4 kHz.

7. Conclusion

In order to maintain high sensitivity, the proof mass has a low resonant frequency and a high quality factor. On small input signal approximations, the tunneling accelerometer model is analyzed and linearized. The relationships of control systems, open loop systems, and close loop systems are derived. Based on this approximation, a simple but effective means to synthesize a control system is successively exerted so that the close loop system has broadened the bandwidth and optimized

damping while maintaining its high sensitivity. The analysis of gain and phase margin, root locus, and pole distribution show that the system is a stable system.

A model of a tunneling accelerometer sensor is constructed with MatLab Simulink. All the tunneling accelerometer functions, such as dynamic range, output voltage dependent input acceleration, exponential response of tunneling current, and frequency response of measurement, are simulated and plotted.

Acknowledgments

This work is partially supported by NSF EPS-0092001, LEQSF (2001-04)-RII-02, and the NASA (2002)-Stennis-22 Foundation.

References

[1] Quate C F *et al* 1998 Tunneling accelerometer *J. Microscopy* **152** 73–6

[2] Waltman S B and Kaiser W J 1989 An electron tunneling sensor *Sensors Actuators* **19** 201–10

[3] Kenny T W, Waltman S B, Reynolds J K and Kaiser W J 1991a Micro-machined silicon tunneling sensor for motion detection *Appl. Phys. Lett.* **58** 100–2

[4] Liu C H, Grade J D, Barzilai A M, Reynolds J K, Partridge A, Rockstad H K and Kenny T W 1997 Characterization of a High-sensitivity micro machined tunneling accelerometer *Transducers'97, Int. Conf. on Solid-State Sensors and Actuators (Chicago, 16–19 June)* pp 471–2

[5] Hartwell P G, Bertsch F M, Miller S A, Turner K L and MacDonald N C 1998 Single mask lateral tunneling accelerometer *Proc. IEEE Micro Electro Mechanical Systems Workshop (MEMS'98)* pp 340–4

[6] Grade J D, Barzilai A M, Reynolds J K, Liu C-H, Partridge A, Miller L M, Podosek J A and Kenny T W 1997 Low frequency drift in tunneling sensors *Transducers'97, Int. Conf. on Solid-State Sensors and Actuators (Chicago, 16–19 June)* pp 871–4

[7] Liu C-H, Rockstad H K and Kenny T W 1999 Robust controller de-sign via μ-synthesis for high-performance micro machined tunneling accelerometers *Proc. 1999 American Control Conference* pp 247–52

[8] Liu C-H and Kenny T W 2001 A high-precision wide-bandwidth micro machined tunneling accelerometer *J. Microelectromech. Syst.* **10** 425–33

[9] Yeh C and Najafi K 1998 CMOS interface circuitry for a low-voltage micro machined tunneling accelerometer *J. Microelectromech. Syst.* **7** 6–15

[10] Wang J, McClelland B, Zavracky P M, Hartley F and Dolgin B 1996 Design, fabrication and measurement of a tunneling tip accelerometer *Proc. Solid-State Sensor and Actuator Workshop (Hilton Head, SC)* pp 68–71

[11] Kubena R L, Atkinson G M, Robinson W P and Stratton F P 1996 A new miniaturized surface micro machined tunneling accelerometer *IEEE Electron Device Lett.* **17** 306–8

[12] Liu C-H, Barzilai A M, Reynolds J K, Partridge A, Kenny T W, Garde J D and Rockstad H K 1998 Characterization of a high-sensitivity micro machined tunneling accelerometer with micro-g resolution *J. Microelectromech. Syst.* **7** 235–44

[13] Rockstad H K, Tang T K, Reynolds J K, Kenny T W, Kaiser W J and Gabrielson T B 1996 A miniature high-sensitivity electron tunneling accelerometer *Sensors Actuators* A **53** 227

[14] Liu C H, Reynolds J K, Partridge A, Grade J D, Barzilai A M, Kenny T W and Rockstad H K 1997 A high-sensitivity micro machined accelerometer based on electron tunneling transducers in *Proc. ASME Winter Conference—Symposium on Micro Electro Mechanical Systems (Dallas, TX)* pp 13–20